Supplement of Solid Earth, 11, 627–655, 2020
https://doi.org/10.5194/se-11-627-2020-supplement

Solid Earth
Open Access

Supplement of

Influence of reservoir geology on seismic response during decameter-scale hydraulic stimulations in crystalline rock

Linus Villiger et al.

Correspondence to: Linus Villiger (linus.villiger@sed.ethz.ch)

Section S1: Seismic event detection

The following figures show evolution of event detection of all experiments, additionally to flow rate and injection pressure. The color-coded area represents the contribution of events according to their detection within the borehole sensor array (i.e., events recorded on all eight borehole sensors correspond to a coincidence level of eight). The strips on top of the "cumulative number of events" line indicate performed seismic surveys during which passive event detection was on hold.

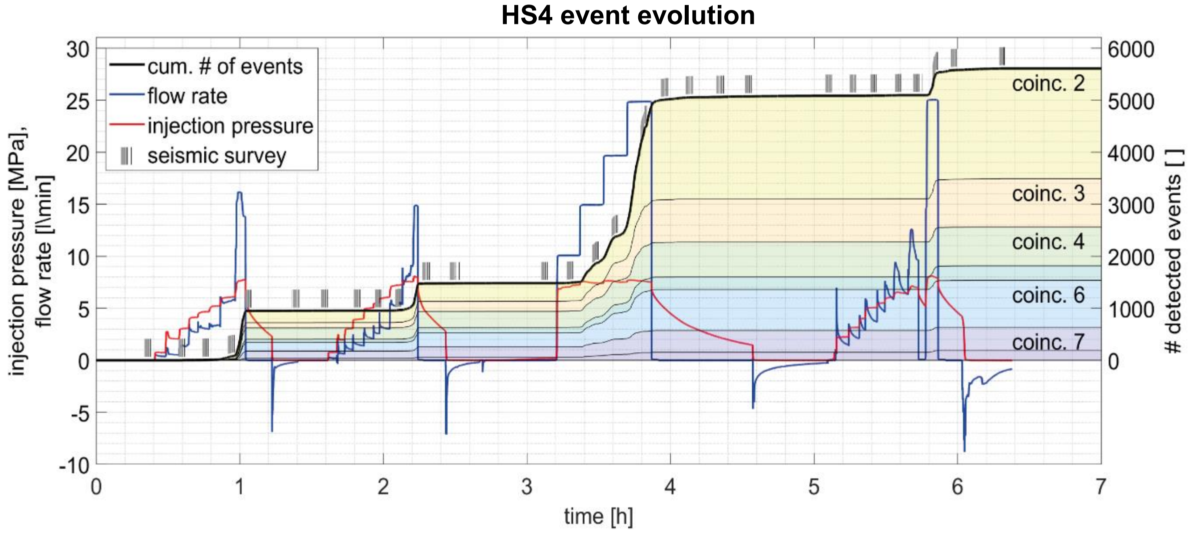

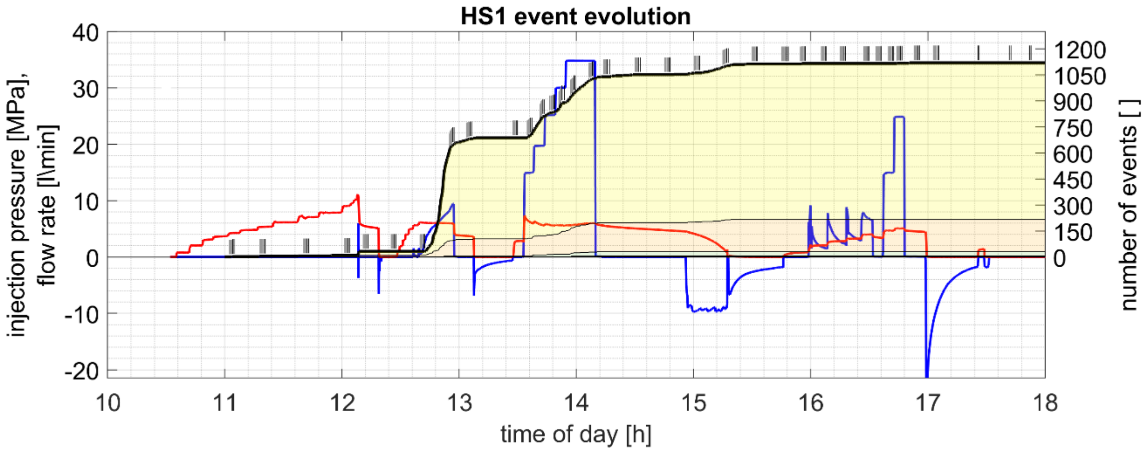

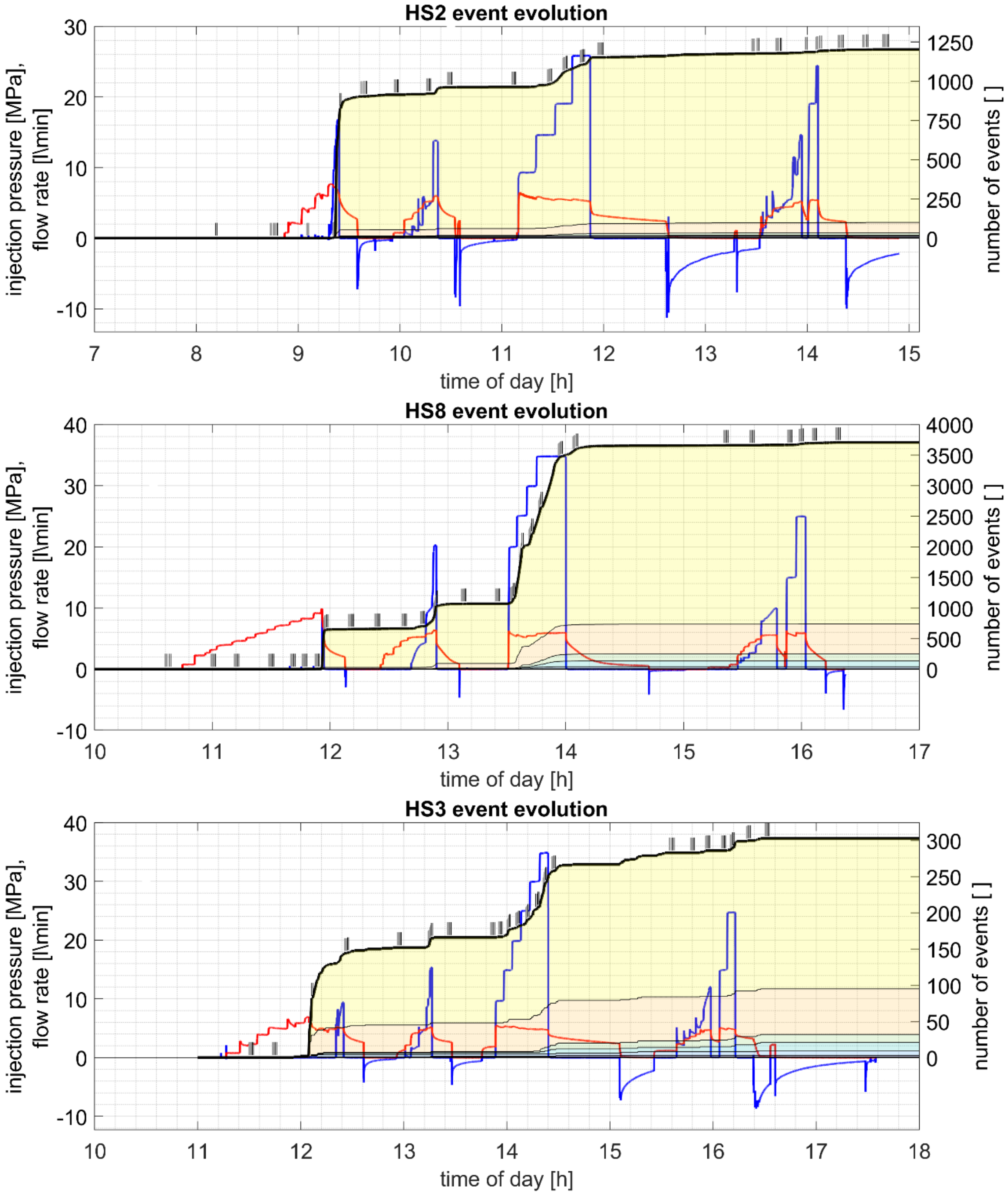
HS2 event evolution
injection pressure [MPa],
flow rate [l\min]
number of events [ ]
time of day [h]
HS8 event evolution
injection pressure [MPa],
flow rate [l\min]
number of events [ ]
time of day [h]
HS3 event evolution
injection pressure [MPa],
flow rate [l\min]
number of events [ ]
time of day [h]

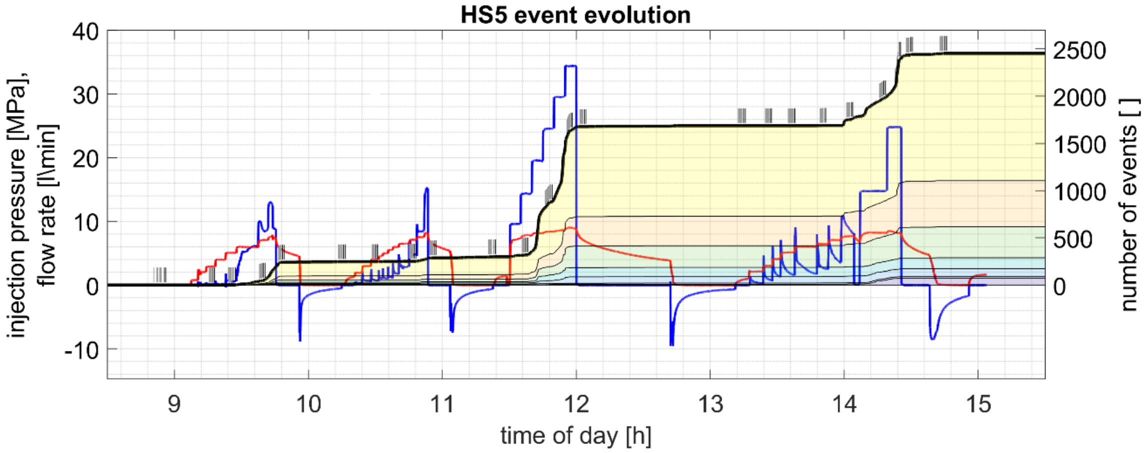
HS5 event evolution
injection pressure [MPa],
flow rate [l\min]
number of events [ ]
time of day [h]
40
30
20
10
0
-10
2500
2000
1500
1000
500
0
9
10
11
12
13
14
15

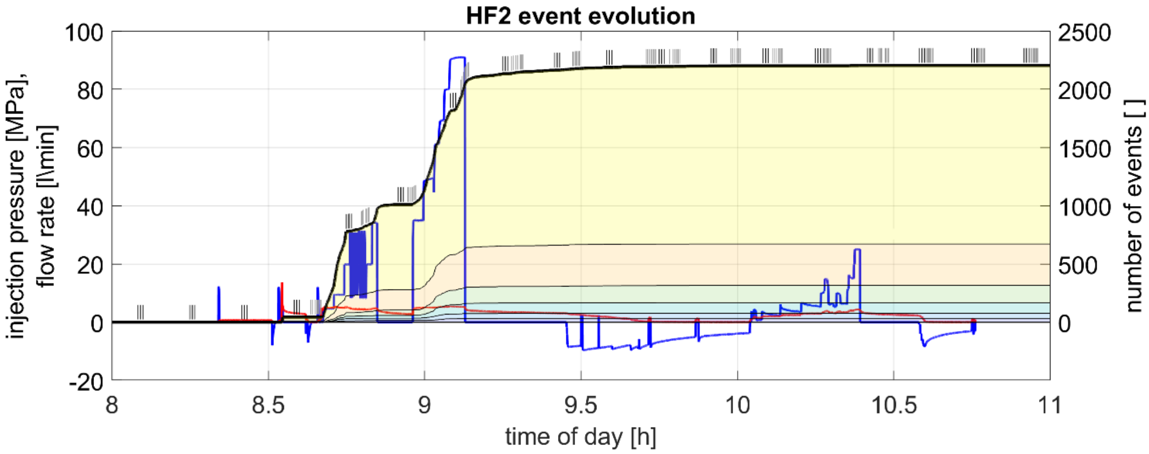
HF2 event evolution
injection pressure [MPa],
flow rate [l\min]
number of events [ ]
time of day [h]
100
80
60
40
20
0
-20
2500
2000
1500
1000
500
0
8
8.5
9
9.5
10
10.5
11

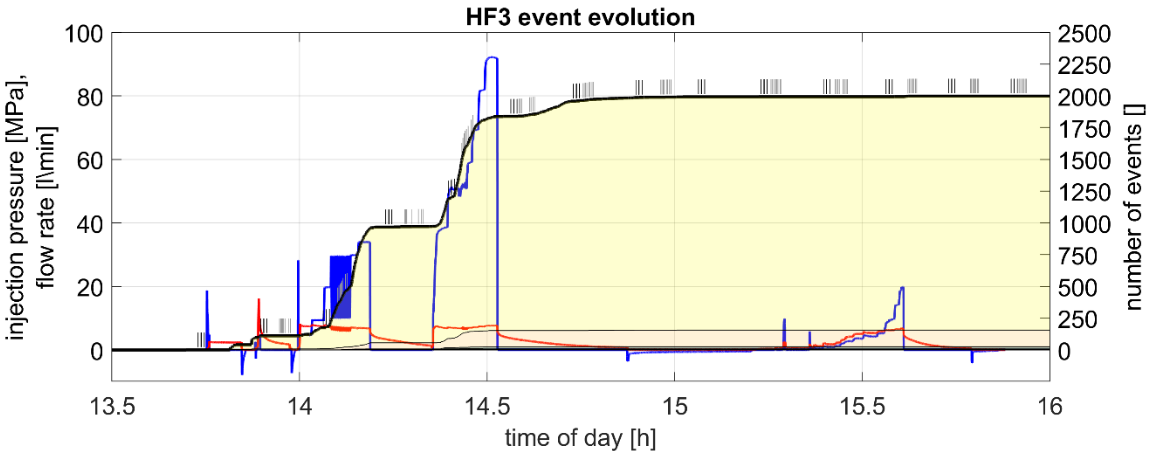
HF3 event evolution
injection pressure [MPa],
flow rate [l\min]
number of events []
time of day [h]
100
80
60
40
20
0
2500
2250
2000
1750
1500
1250
1000
750
500
250
0
13.5
14
14.5
15
15.5
16

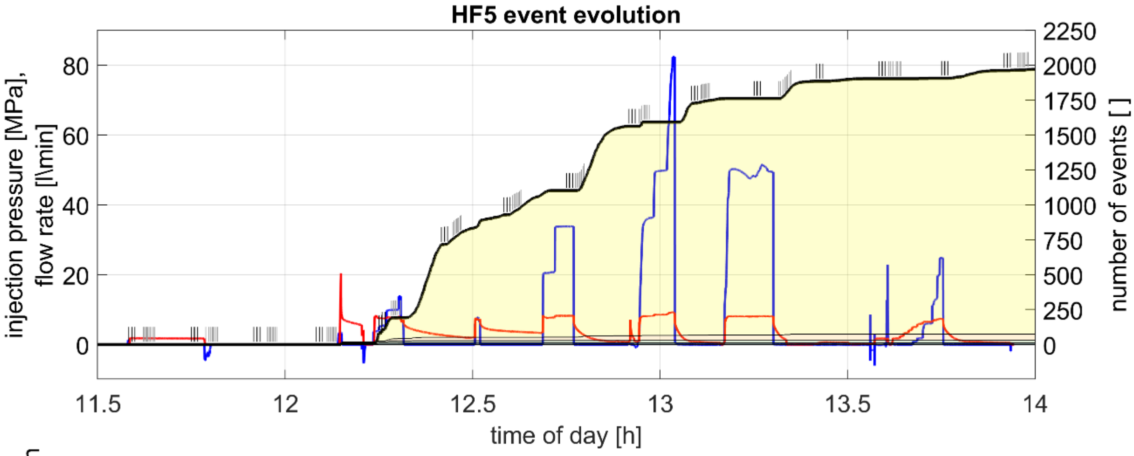
HF5 event evolution
injection pressure [MPa],
flow rate [l\min]
number of events [ ]
time of day [h]
0
20
40
60
80
0
250
500
750
1000
1250
1500
1750
2000
2250
11.5
12
12.5
13
13.5
14

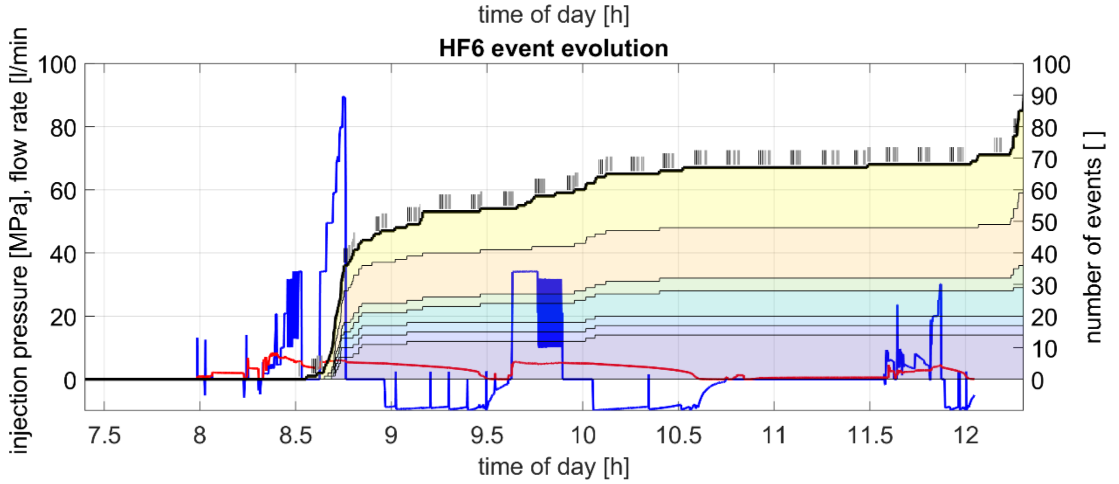
HF6 event evolution
injection pressure [MPa], flow rate [l/min
number of events [ ]
time of day [h]
0
20
40
60
80
100
0
10
20
30
40
50
60
70
80
90
100
7.5
8
8.5
9
9.5
10
10.5
11
11.5
12

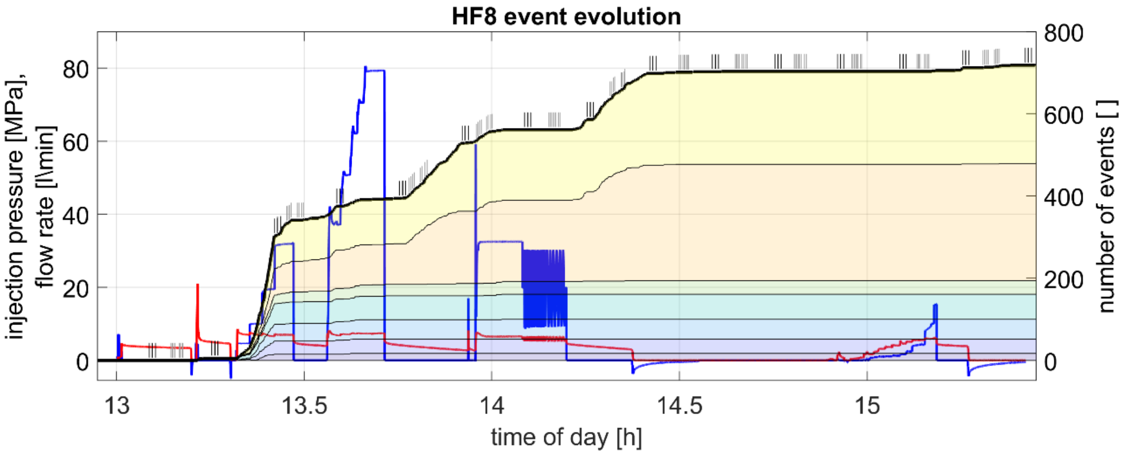
HF8 event evolution
injection pressure [MPa],
flow rate [l\min]
number of events [ ]
time of day [h]
0
20
40
60
80
0
200
400
600
800
13
13.5
14
14.5
15

Section S2: Magnitude correction

The following figure shows a) the estimate of angle dependency on M_R, (b) the estimate of M_R correction due to variations in the coupling quality, (c) instrument responses referenced to velocity for the five piezosensors which are paired with an accelerometer.

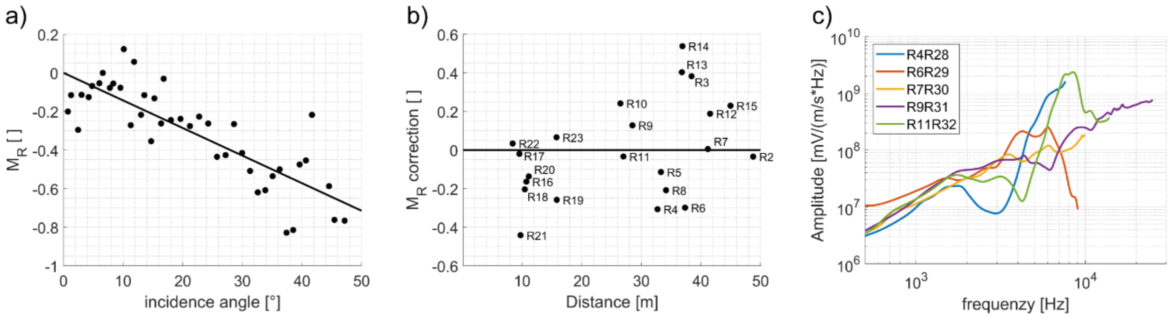

Section S3: Temporal seismic event evolution

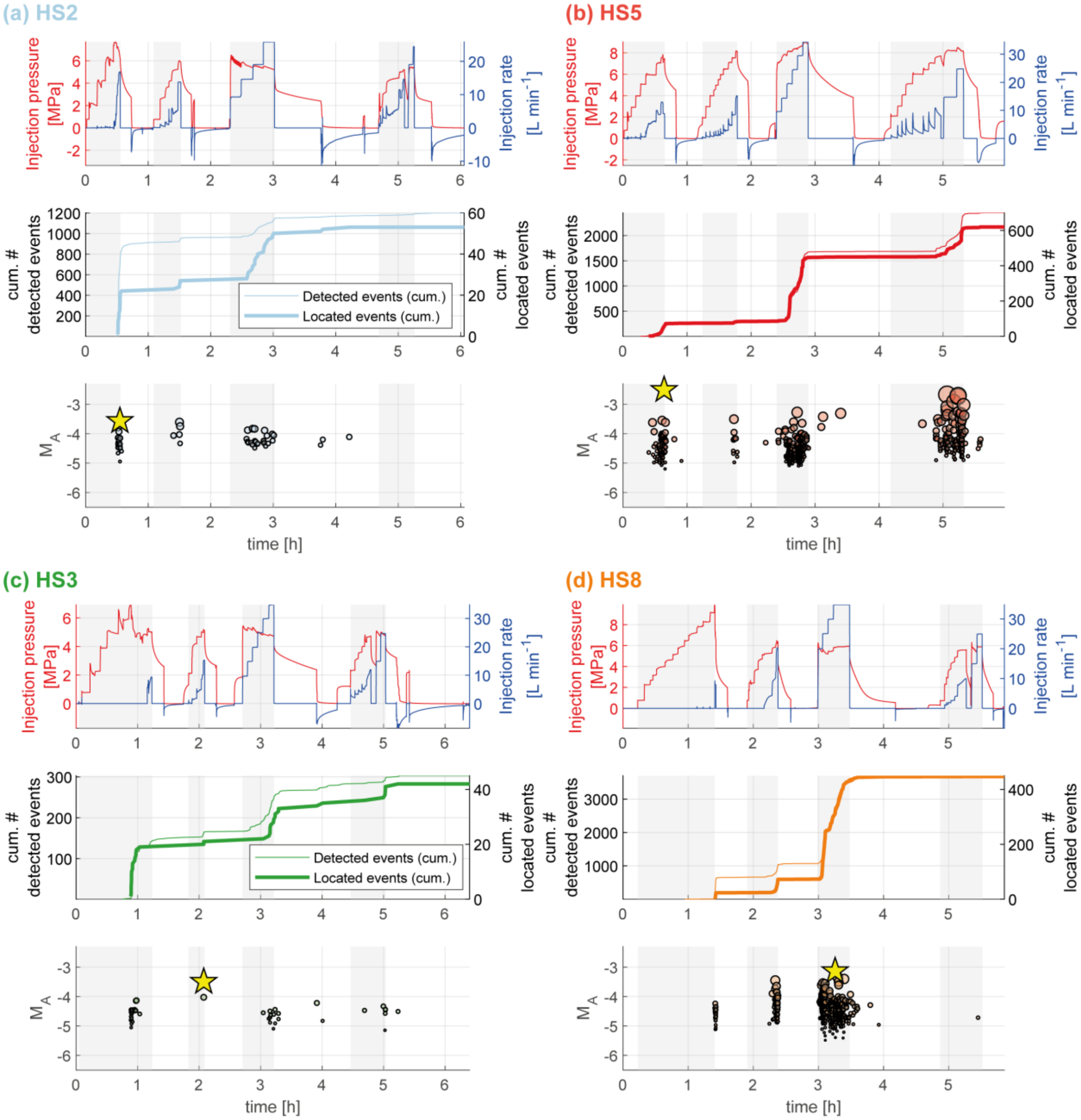

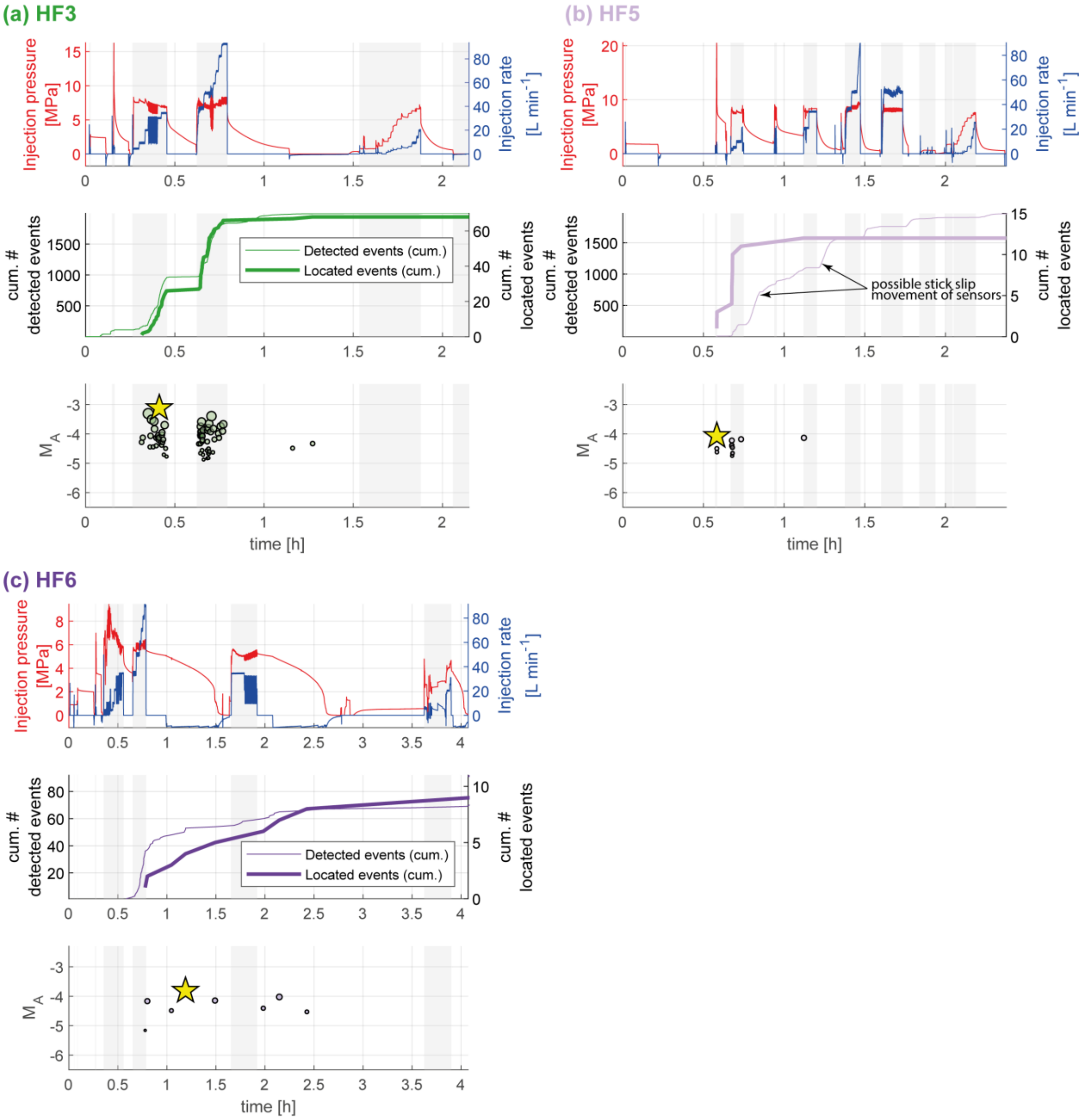
(a) HF3
(b) HF5
(c) HF6
Injection pressure [MPa]
Injection rate [L min-1]
cum. # detected events
cum. # located events
Detected events (cum.)
Located events (cum.)
possible stick slip movement of sensors
M_A
time [h]

Section S4: Plane fits to seismic clouds

Table S4: Orientation of plane fits through seismic clouds (azimuth, dip) along with the standard deviation of positive and negative orthogonal distances to the fitted planes

Injection	**Azimuth [°]**	**Dip [°]**	**σ_{dist} [m]**	**Injection**	**Azimuth [°]**	**Dip [°]**	**σ_{dist} [m]**
HS1	322	89	-1.4 / 1.4	**HF2 – C1**	29	83	-0.3 / 0.5
HS2	175	90	-1.1 / 0.7	**HF2 – C2**	175	76	-0.3 / 0.3
HS3	164	70	-0.4 / 0.1	**HF3**	-	-	-
HS4 – C1	169	76	-0.1 / 0.1	**HF5**	17	73	-0.3 / 0.2
HS4 – C2	6	82	-0.1 / 0.2	**HF6**	-	-	-
HS4 – C3	30	45	-0.2 / 0.2	**HF8**	178	70	-0.4 / 0.5
HS5	172	81	-0.9 / 1.2				
HS8	181	79	-0.6 / 0.9				

Section S5: Estimate of seismically activated area

The planes fitted through the seismicity cloud allow an estimate of the an upper (convex hull) and lower bound (concave hull) of seismically activated area (Table S5) and its temporal evolution. The upper bound of the seismically activated area was estimated based on boundary edges (convex hull) surrounding the collapsed seismic events (Barber et al., 1996). For the lower bound, the seismically activated area was inferred using an estimate based on the concave hull after Gurram et al. (2007) using a lambda parameter of 0.5. The largest area (convex hull) was activated during injection experiment HS5 and amounts in almost 300m2.

In general, for all the HS injection experiments, the seismically active area during the actual stimulation cycle (C3), where about 50% of the total volume per injection was pumped, is the largest. Injection experiments HS1, HS2 and HS3 performed on S1 shear zones reveal overlapping seismically-activated areas, which is interpreted as repeated rupturing on seismically active patches. Injection HS2 shows ongoing seismicity around the injection interval, and in injection HS3 the seismicity cloud changes from an upward migration (cycle 1) towards a migration direction facing downwards (cycle 3, 4). In injection HS1, seismicity clouds migrate upwards in a consecutive fashion. Injection experiments HS5, HS4 and HS8 performed on S3 structures are the experiments where the seismically activated area was highest (among the HS injection experiments). In experiment HS5 and HS8, injection borehole INJ1 was hydraulically connected to injection borehole INJ2. In experiment HS5 the seismic events induced during cycles 1, 2 formed around the injection interval in INJ1 in an upward facing direction. In cycle 3 seismicity migrated further upwards, towards the East. In cycle 4, the seismicity cloud changed its migration direction downwards, arriving at the injection borehole INJ2 (more information on injection experiment HS5 can be found in Krietsch et al. (in preparation)).

Injection experiment HS8 was performed in an interval that includes an S1 structure south of the S3 shear zones. During injection cycle 1, only the area around injection borehole INJ1 was seismically activated. In cycle 2, seismicity further migrated towards the East in the direction of the injection borehole INJ2. During injection cycle 3, injection boreholes INJ1 and INJ2 were definitely hydraulically connected. In addition, seismicity occurs in the lower regions of shear zone S3.1.

Injection experiment HS4, with over 50% of located seismic events from all injection experiments, is contained in a comparatively small volume. The seismicity clouds induced during injection experiment HS4 formed in the metabasic dykes (cluster 1) and the pre-existing fractures (cluster 2) and show a very high density of seismicity around the injection interval over all injection cycles, providing evidence of repeated rupturing on seismically active patches. A new seismicity cloud induced in cycle 3 formed perpendicular to the minimum principal stress of the perturbed stress state in an Easterly direction over a time period of 12 minutes and reopened in injection cycle 4.

Table S5: Upper and lower bound of the seismically activated area from all injection experiments, where a plane fit seemed adequate. Note: The area estimates stem from induced seismic events from all cycles. Repeated seismicity on seismically active patches do not add to the seismically activated area estimate.

Injection	Lower bound (concave hull) [m^2]	Upper bound (convex hull) [m^2]	Injection	Lower bound (concave hull) [m^2]	Upper bound (convex hull) [m^2]
HS1	102.1	172.6	**HF2**	66.0	123.1
HS2	33.6	104.4	**HF3**	-	-
HS3	74.2	121.6	**HF5**	6.8	9.1
HS4	141.8	279.8	**HF6**	-	-
HS5	224.3	345.2	**HF8**	160.5	310.8
HS8	120.6	183.0			

Hydraulic fracturing experiments HF5 and HF8, both performed south of shear zones S3 in close proximity to each other, could not be more different in terms of seismically activated areas. Injection HF5 activated a comparably small area, with activated areas over cycles overlapping. Experiment HF8, on the other hand, activated a larger area; seismicity begins to light up in the formation breakdown cycle in close proximity to the injection interval, followed by a significant area gain during the first refrac cycle surrounding the injection interval. The seismicity clouds of the subsequent two refrac cycles overlap, suggesting repeated rupturing on seismically active fault patches. The propagation direction of the two refrac cycles is downwards with respect to the injection interval. During injection experiment HF2, the first seismic events are located at the beginning of refrac 2 in close proximity to the injection interval in borehole INJ1 (start of cluster 1). The initiated seismic events orient themselves in parallel to the injection interval axis, in a direction perpendicular to the minimum principal stress of the perturbed stress state. During the subsequent flow controlled refrac cycle 3, the seismically activated area of cluster 1 increases, and a new seismicity cloud forms in an East-West orientation (cluster 2). In cluster 1, during refrac cycles 4 and 5, seismicity clouds overlay the seismicity induced during cycle 2 and 3. During cycle 4, cluster 2 is enlarged in the planar East-West direction. The seismicity cloud induced during cycle 5 overlays seismicity of the previous cycles in cluster 2.

a. Seismically activated area estimates HS experiments

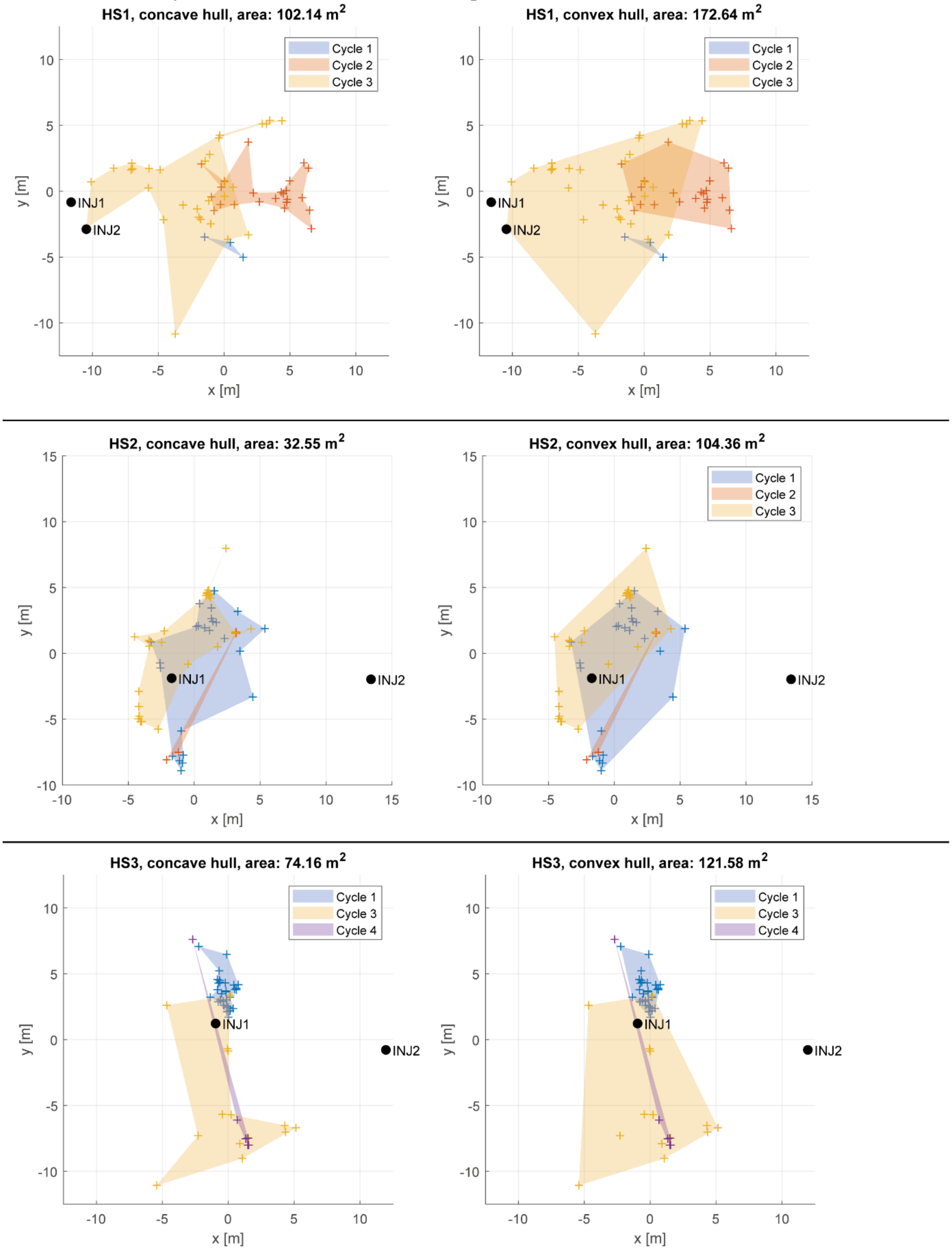

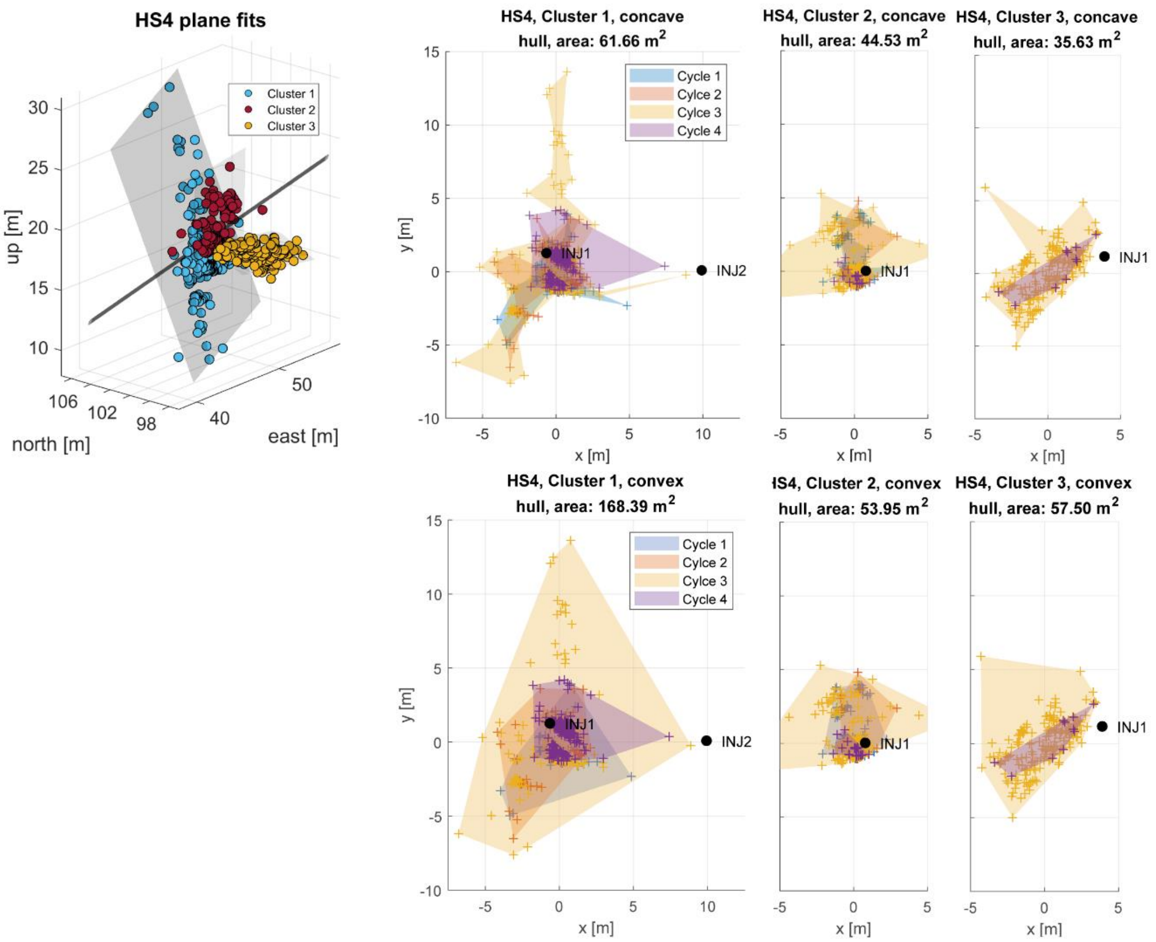
HS4 plane fits
Cluster 1
Cluster 2
Cluster 3
up [m]
north [m]
east [m]
HS4, Cluster 1, concave hull, area: 61.66 m2
HS4, Cluster 2, concave hull, area: 44.53 m2
HS4, Cluster 3, concave hull, area: 35.63 m2
Cycle 1
Cylce 2
Cylce 3
Cycle 4
INJ1
INJ2
y [m]
x [m]
HS4, Cluster 1, convex hull, area: 168.39 m2
HS4, Cluster 2, convex hull, area: 53.95 m2
HS4, Cluster 3, convex hull, area: 57.50 m2

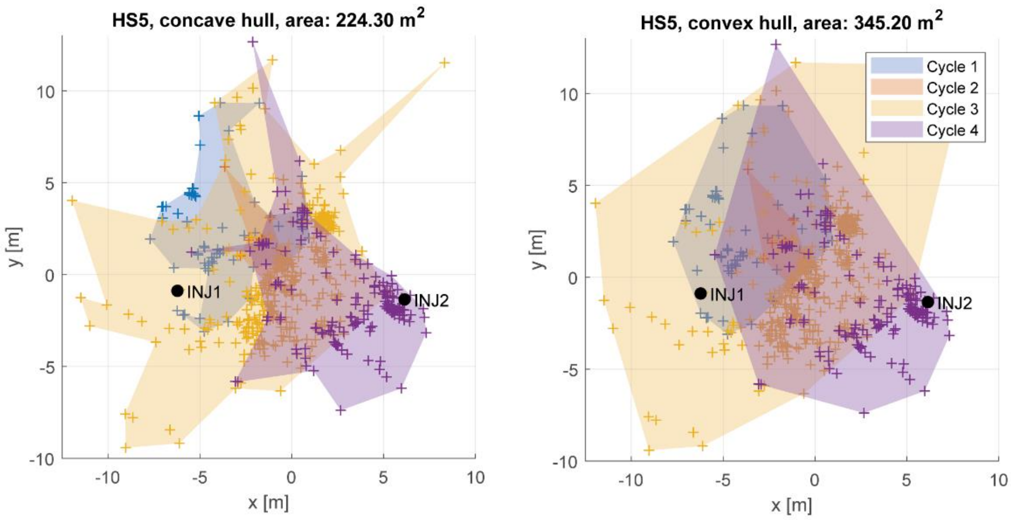
HS5, concave hull, area: 224.30 m2
HS5, convex hull, area: 345.20 m2
Cycle 1
Cycle 2
Cycle 3
Cycle 4
INJ1
INJ2
y [m]
x [m]

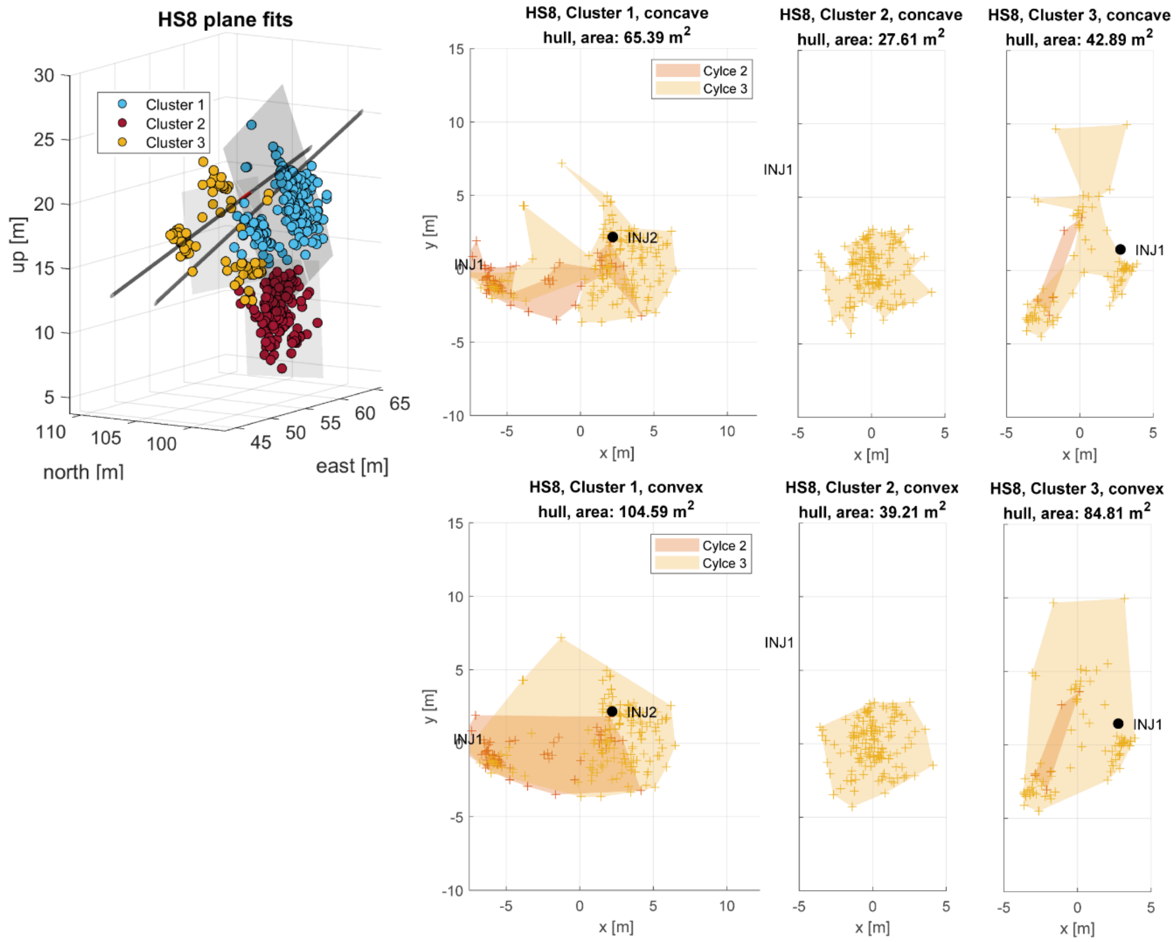
HS8 plane fits
Cluster 1
Cluster 2
Cluster 3
up [m]
north [m]
east [m]
HS8, Cluster 1, concave hull, area: 65.39 m2
HS8, Cluster 2, concave hull, area: 27.61 m2
HS8, Cluster 3, concave hull, area: 42.89 m2
HS8, Cluster 1, convex hull, area: 104.59 m2
HS8, Cluster 2, convex hull, area: 39.21 m2
HS8, Cluster 3, convex hull, area: 84.81 m2
Cylce 2
Cylce 3
INJ1
INJ2
x [m]
y [m]

b. Seismically activated area estimates HF experiments

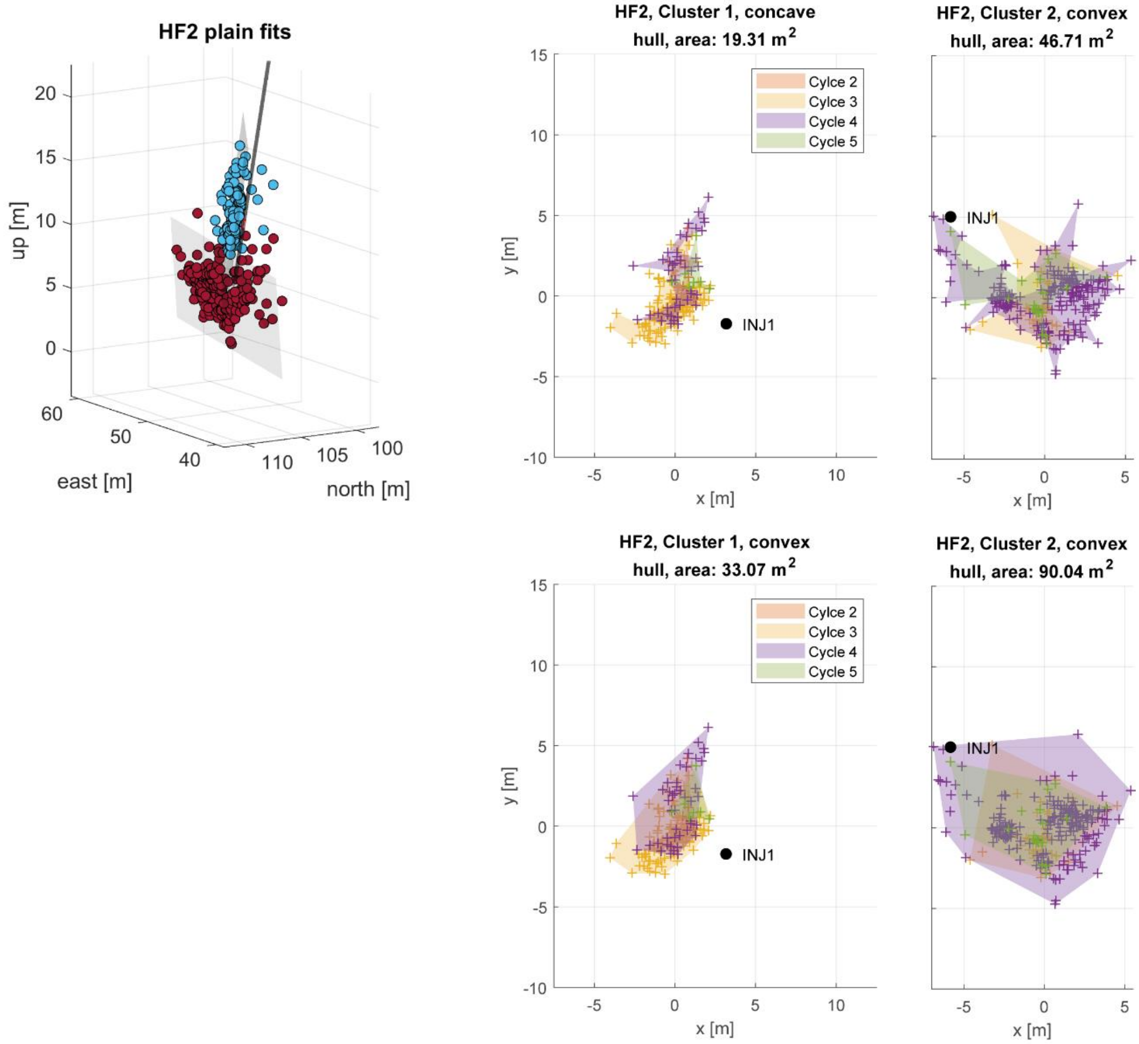

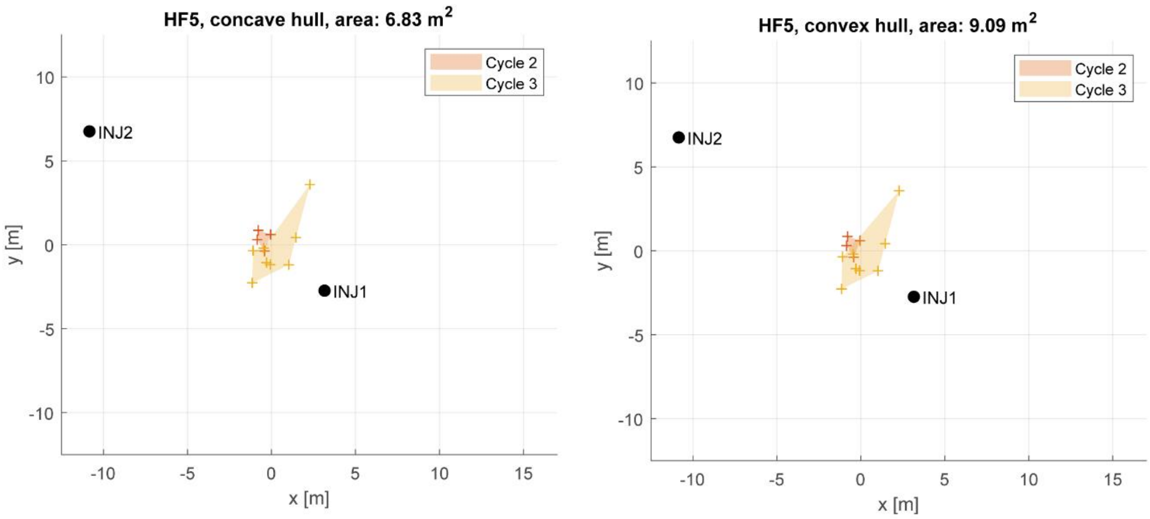

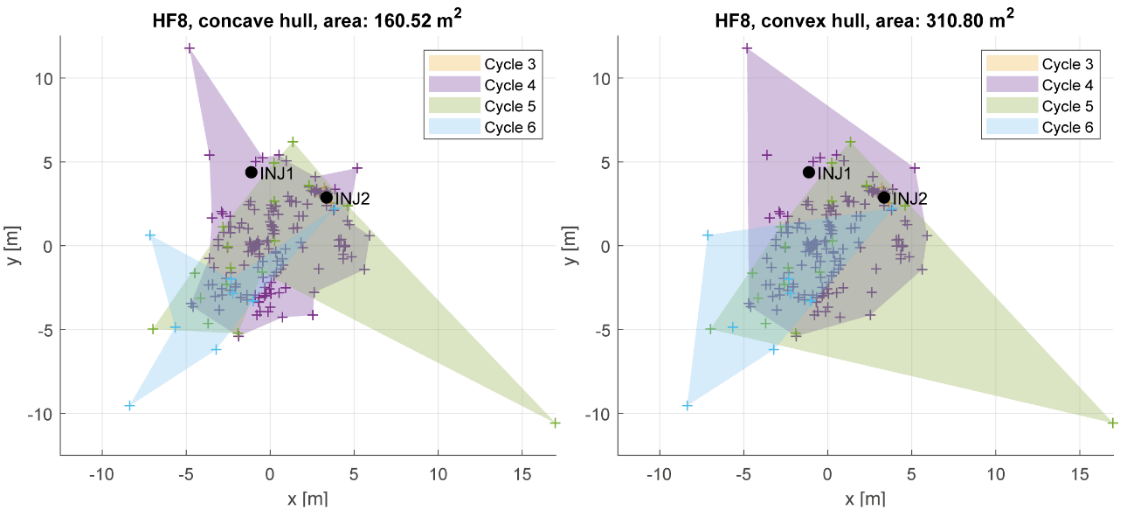
HF8, concave hull, area: 160.52 m2
Cycle 3
Cycle 4
Cycle 5
Cycle 6
INJ1
INJ2
y [m]
x [m]
HF8, convex hull, area: 310.80 m2
Cycle 3
Cycle 4
Cycle 5
Cycle 6
INJ1
INJ2
y [m]
x [m]

Section S6: Estimates of seismic triggering fronts

Diffusivity values were derived from time-distance representations of seismicity based on the concept of seismic triggering fronts in a homogeneous, isotropic and poroelastic medium introduced by Shapiro et al. (2002). The distance of the seismicity front to the injection interval is $r = \sqrt{4\pi Dt}$, where D is the scalar hydraulic diffusivity in $\frac{m^2}{s}$ and t is the time from the beginning of injection. The time from the beginning of injection was substituted with $t = \frac{\Delta V_{cycle}}{mean(Q)_{cylce}}$, where ΔV_{cycle} is the injected cumulative volume per cycle and $mean(Q)_{cylce}$ represents the mean flow rate of the respective cycle.

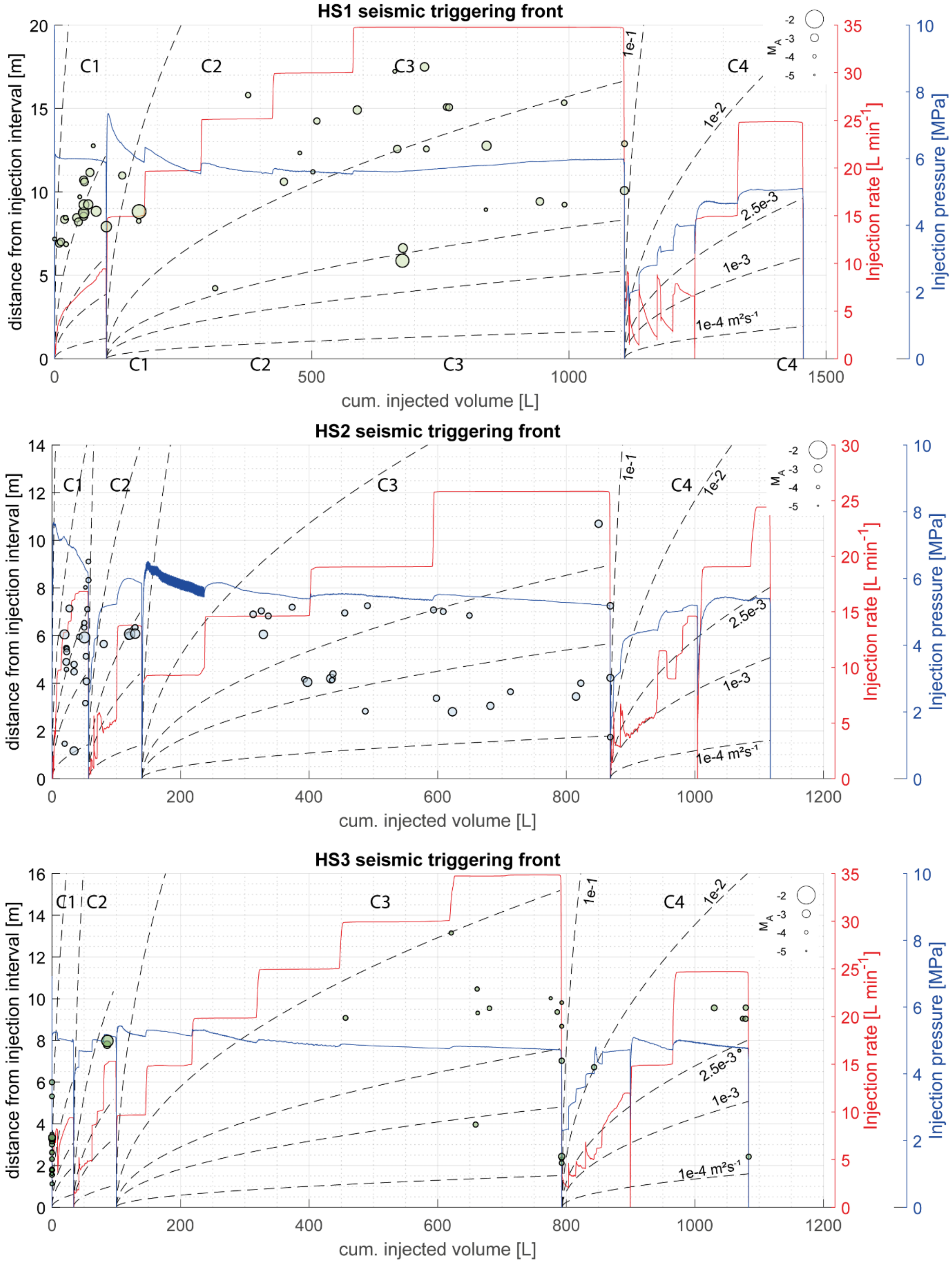
HS1 seismic triggering front
distance from injection interval [m]
cum. injected volume [L]
Injection rate [L min-1]
Injection pressure [MPa]
C1
C2
C3
C4
1e-1
1e-2
2.5e-3
1e-3
1e-4 m²s-1
MA
HS2 seismic triggering front
HS3 seismic triggering front

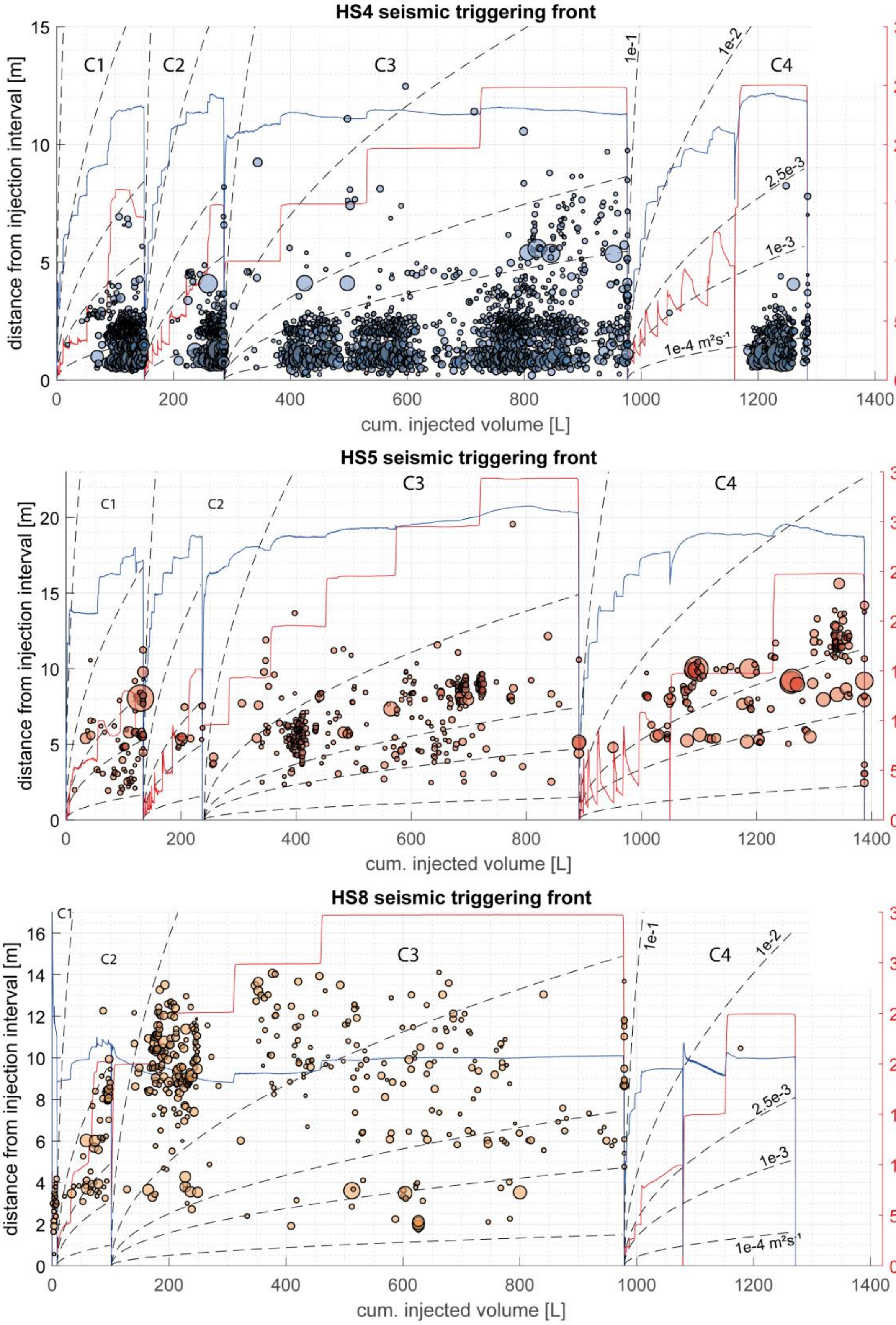
HS4 seismic triggering front
distance from injection interval [m]
cum. injected volume [L]
Injection rate [L min-1]
Injection pressure [MPa]
C1
C2
C3
C4
1e-1
1e-2
2.5e-3
1e-3
1e-4 m²s-1
HS5 seismic triggering front
distance from injection interval [m]
cum. injected volume [L]
Injection rate [L min-1]
Injection pressure [MPa]
C1
C2
C3
C4
HS8 seismic triggering front
distance from injection interval [m]
cum. injected volume [L]
Injection rate [L min-1]
Injection pressure [MPa]
C1
C2
C3
C4
1e-1
1e-2
2.5e-3
1e-3
1e-4 m²s-1

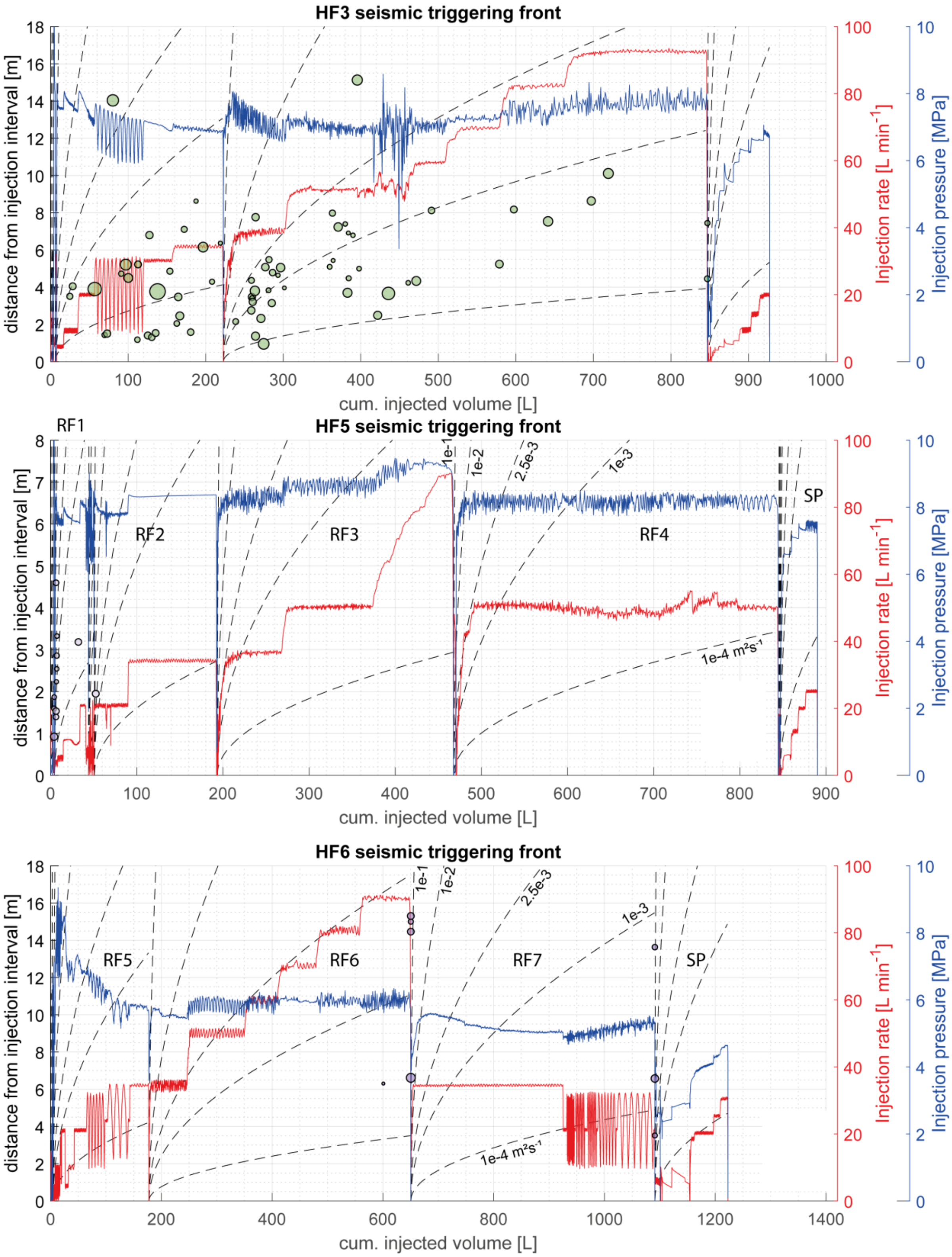
HF3 seismic triggering front
distance from injection interval [m]
Injection rate [L min-1]
Injection pressure [MPa]
cum. injected volume [L]
RF1
HF5 seismic triggering front
1e-1
1e-2
2.5e-3
1e-3
1e-4 m²s-1
RF2
RF3
RF4
SP
HF6 seismic triggering front
RF5
RF6
RF7
SP
1e-1
1e-2
2.5e-3
1e-3
1e-4 m²s-1

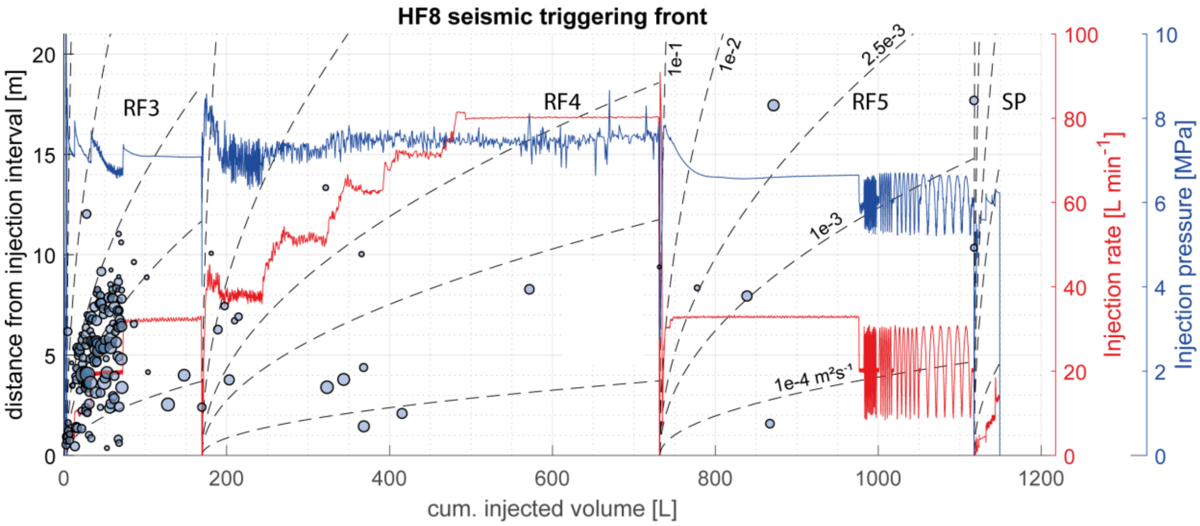
HF8 seismic triggering front
distance from injection interval [m]
cum. injected volume [L]
Injection rate [L min-1]
Injection pressure [MPa]
RF3
RF4
RF5
SP
1e-1
1e-2
2.5e-3
1e-3
1e-4 m²s-1

Section S7: Moment magnitude M_W vs. amplitude magnitude M_A

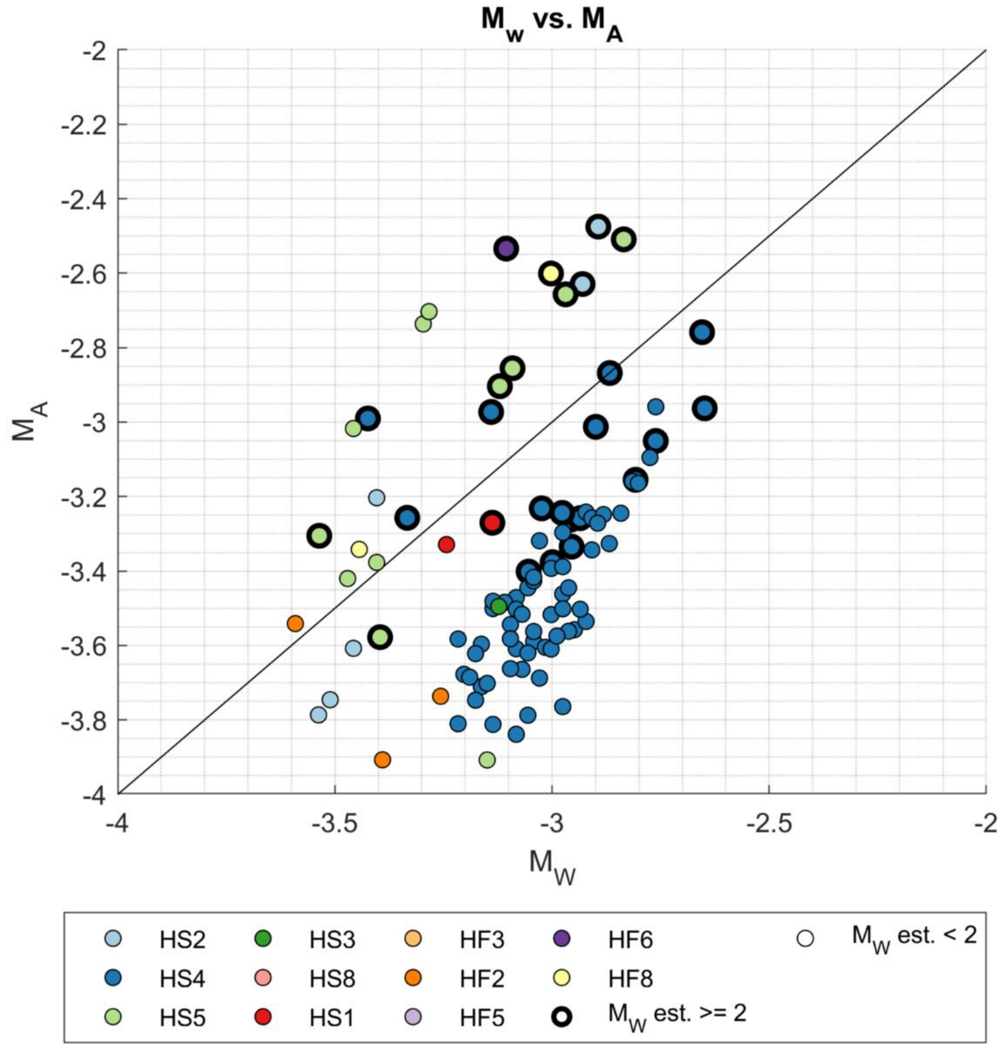

Figure S7: M_W estimates throughout all experiments and the corresponding amplitude magnitude M_A calculated from relative magnitudes M_r using $M_A = M_r - 4.0$. The linear relationship between M_r and M_A was determined using the mean value of the differences between M_r and M_W, as well as assuming a slope of one. For the calculation, only events exhibiting more than two M_W estimates were considered (circles with think linewidth).

Section S8: a) Located seismic events resolved in cycles and phases of all HS experiments

Phase	**start-shut-in**	**shut-in – venting**	**venting-start**	**start-shut-in**	**shut-in – venting**	**venting-start**	**venting-start**	**start-shut-in**	**shut-in – venting**	**venting-start**	**start-shut-in**	**shut-in – venting**
Cycle	**C1**	**C1**	**C1**	**C2**	**C2**	**C2**	**C3**	**C3**	**C3**	**C4**	**C4**	**C4**
HS1	3	0	0	22	1	0	27	1	2	0	0	0
HS2	29	1	0	6	0	0	24	1	2	0	0	0
HS3	29	0	1	2	0	0	8	4	2	6	0	1
HS4	678	5	0	375	9	2	1656	25	1	330	23	5
HS5	62	12	1	8	2	1	367	4	0	169	4	4
HS8	0	23	0	50	0	0	364	13	0	1	0	0
Events during stimulation	4216											
Events between shut-in and venting	128											
Events between venting and new cycle	22											

b) Located seismic events resolved in cycles and phases of all HF experiments

F – Formation break down cycle
RF – Refrac cycle
SP – Step pressure injection

HF2	**F**	**Start RF1**	**Shut-in RF1**	**Venting RF1**	**Start RF2**	**Shut-in RF2**	**Start RF3**	**Shut-in RF3**	**Venting RF3**	**Start SP**	**Shut-in SP**	**Venting SP**
Nr.	0	11	0	0	201	7	272	23	7	0	0	0

HF3	**F**	**Start RF1**	**Shut-in RF1**	**Venting RF1**	**Start RF2**	**Shut-in RF2**	**Start RF3**	**Shut-in RF3**	**Venting RF3**	**Start SP**	**Shut-in SP**	**Venting SP**
Nr.	0	0	0	0	26	0	42	0	2	0	0	0

HF5	**F**	**Start RF1**	**Shut-in RF1**	**Venting RF1**	**Start RF2**	**Shut-in RF2**	**Venting RF2**	**Start RF3**	**Shut-in RF3**	**Start RF4**	**Shut-in RF4**	**Start SP**	**Shut-in SP**	**Venting SP**
Nr.	0	4	0	0	9	0	0	0	0	0	0	0	0	0

HF6	F	Start RF1	Shut-in RF1	Start RF2	Shut-in RF2	Start RF3	Shut-in RF3	Venting RF3	Start RF4	Shut-in RF4	Venting RF4	Start RF5	Shut-in RF5	Start RF6	Shut-in RF6	Venting RF6	Start RF7	Shut-in RF7	Venting RF7	Start SP	Shut-in SP	Venting SP
Nr.	0	0	0	0	0	0	0	0	0	0	0	0	0	1	2	3	0	5	2	0	0	0

HF8	F	Start RF1	Shut-in RF1	Venting RF1	Start RF2	Shut-in RF2	Venting RF2	Start RF3	Shut-in RF3	Start RF4	Shut-in RF4	Start RF5	Shut-in RF5	Venting RF5	Start SP	Shut-in SP	Venting SP
Nr.	0	0	0	0	2	1	0	155	1	16	2	6	3	0	0	0	0

Events during stimulation	746
Events between shut-in and venting	44
Events between venting and new cycle	0

Referneces

Barber, C. B., Dobkin, D. P., and Huhdanpaa, H.: The quickhull algorithm for convex hulls, ACM Transactions on Mathematical Software (TOMS), 22, 469-483, 1996.

Gurram, P., Lach, S., Saber, E., Rhody, H., and Kerekes, J.: 3d scene reconstruction through a fusion of passive video and lidar imagery, 36th Applied Imagery Pattern Recognition Workshop (aipr 2007), 2007, 133-138,

Krietsch, H., Villiger, L., Doetsch, J., Gischig, V., Evans, K., Brixel, B., Jalali, M., Loew, S., and Amann, F.: Interplay between Hydraulic Shearing and Hydraulic Fracturing observed during an In-Situ Hydraulic Stimulation Expriement, in preparation.

Shapiro, S. A., Rothert, E., Rath, V., and Rindschwentner, J.: Characterization of fluid transport properties of reservoirs using induced microseismicity, Geophysics, 67, 212-220, 2002.